Journal of Alloys and Compounds 515 (2012) 114–118

Contents lists available at SciVerse ScienceDirect

Journal of Alloys and Compounds

journal homepage: www.elsevier.com/locate/jallcom

Martensitic transformation and magnetocaloric effect in Mn–Ni–Nb–Sn shape memory alloys: The effect of 4d transition-metal doping

Zhida Han[a,b,c,*], Xi Chen[a], Yao Zhang[a], Jie Chen[a], Bin Qian[a,b], Xuefan Jiang[a,b], Dunhui Wang[c], Youwei Du[c]

[a] Department of Physics, Changshu Institute of Technology, Changshu 215500, People's Republic of China
[b] Jiangsu Laboratory of Advanced Functional Materials, Changshu Institute of Technology, Changshu 215500, People's Republic of China
[c] Department of Physics, Nanjing University, Nanjing 210093, People's Republic of China

ARTICLE INFO

Article history:
Received 30 September 2011
Received in revised form
18 November 2011
Accepted 22 November 2011
Available online 30 November 2011

PACS:
75.30.sg

Keywords:
Ferromagnetic shape memory alloy
Martensitic transformation
Magnetocaloric effect

ABSTRACT

The influence of 4d transition-metal Nb substitution for Ni in $Mn_{50}Ni_{50-y}Sn_y$ ($y = 9, 10$) alloys on the phase transitions and magnetocaloric effect was investigated. Austenitic phase of Nb-doped $Mn_{50}Ni_{50-y}Sn_y$ alloys have the cubic structure, and Nb addition results in the expansion of cell volume. The martensitic transformation temperatures decrease with the increase of Nb content, which could be explained by the decrease of valence electron concentration. Our results indicate that 4d transition-metal doping may provide an alternative way to tailor the martensitic transformation and the magnetocaloric effect in ferromagnetic shape memory alloys.

1. Introduction

Ni–Mn–X (X = In, Sn, Sb) based ferromagnetic shape memory alloys, first reported by Sutou et al. in 2004 [1], have attracted increasing interest due to their potential application in magnetic refrigerant, sensor, and actuator. Owing to the strong coupling between the crystal structure and magnetism, these alloys undergo a martensitic transformation (MT) from the parent austenitic phase to the martensitic phase upon cooling, which is often accompanied by the sudden drop of magnetization (ΔM) [2,3]. As a result, under the drive of Zeeman energy $E_{Zeeman} = \mu_0 \Delta M \cdot H$, where H is the strength of applied field, magnetic field induced the transformation from martensitic to austenitic phase can be observed near the MT. This phenomenon makes these alloys exhibit multifunctional properties, such as large magnetocaloric effect (MCE) [4–7], magnetoresistance [8,9], and metamagnetic shape memory effect [10].

In Ni–Mn–X (X = In, Sn, Sb) FSMAs, the MT temperatures can be tuned by alloy composition, preparation condition, and external parameters (magnetic field and hydrostatic pressure [11]). Several factors have been proposed to affect the value of MT temperatures. First, MT temperatures can be tuned by changing the valence electron concentration (e/a) through composition variation or 3d transition metal substitution such as Cr, Fe, Co, Cu [12–15]. Second, cell volume has been proved to have great influence on the transition temperature [16,17]. Third, different grain size, which can be obtained by annealing melt-spun ribbon at different temperatures, produced different MT temperatures [18]. Up to now, although many investigations have focused on the effect of 3d transition-metal doping on the phase transitions and phenomena around MT in Ni–Mn–X (X = In, Sn, Sb) FSMAs, the effect of 4d transition-metal substitution has not been reported. The purpose of this paper is to investigate the influence of 4d metal doping on the phase transitions as well as MCE in high Mn-content $Mn_{50}Ni_{50-x-y}Nb_xSn_y$ alloys and discuss the factors affecting the transition temperatures in these alloy.

2. Experimental

$Mn_{50}Ni_{50-x-y}Nb_xSn_y$ ($x = 0, 1, 2, 3, y = 9$; $x = 0, 1, 2, y = 10$) polycrystalline samples were prepared by arc melting the appropriate amounts of Ni, Mn, Sn and Nb in argon atmosphere. These alloys were sealed in quartz tubes and annealed at 1173 K for 72 h followed by quenching in water. The crystal structures were identified by the X-ray diffraction (XRD) using Cu Kα radiation at room temperature. Thermal behavior was studied using a differential scanning calorimeter (DSC) with the heating and cooling

* Corresponding author at: Department of Physics, Changshu Institute of Technology, Changshu 215500, People's Republic of China. Tel.: +86 512 52899253.
E-mail address: zhida.han@gmail.com (Z. Han).

0925-8388/$ – see front matter © 2011 Elsevier B.V. All rights reserved.
doi:10.1016/j.jallcom.2011.11.102

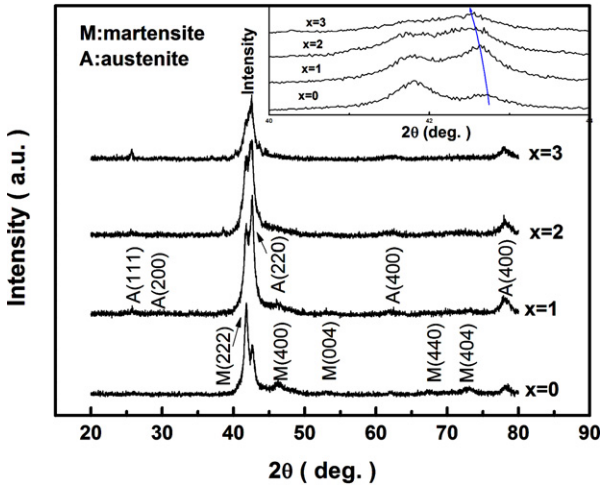

Fig. 1. The XRD patterns of $Mn_{50}Ni_{50-x-y}Nb_xSn_y$ ($x = 0, 1, 2, 3$, $y = 9$) alloys at room temperature. The inset shows the zoom of austenite (2 2 0) peaks.

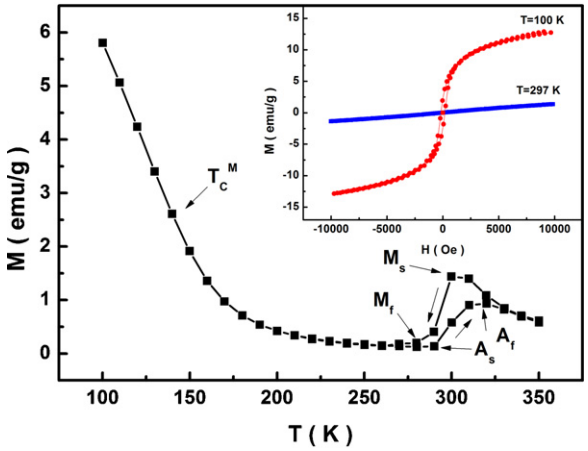

Fig. 2. The temperature dependence of magnetization for $Mn_{50}Ni_{41}Sn_9$ alloys in a magnetic field of 1 kOe on heating and cooling. The inset shows the $M(H)$ loops at 100 and 297 K.

rates of 10 K/min. Magnetic measurements were carried out using a vibrating sample magnetometer (7307, Lakeshore) under a magnetic field up to 10 kOe.

3. Results and discussion

Fig. 1 shows the XRD patterns of $Mn_{50}Ni_{50-x-y}Nb_xSn_y$ ($x = 0$, 1, 2, 3, $y = 9$) alloys at room temperature. The XRD pattern of $Mn_{50}Ni_{41}Sn_9$ illustrates the main martensitic phase of a tetragonal $L1_0$ structure with a minor cubic austenitic structure, indicating the MT temperature is in the vicinity of room temperature. For alloys with $x = 1$ and 2, cubic austenitic phase becomes the main phase with minor phase of $L1_0$ martensite. This means that the substitution of Nb for Ni is favor for the stabilization of austenitic phase, which was confirmed by further increase of Nb content. For alloys with $x = 3$, single cubic austenitic phase can be observed, suggesting that the MT temperature is below room temperature. Previous investigations in Ni–Mn–Sn alloys show that the austenitic phase could be have a cubic $L2_1$ structure ($Fm\bar{3}m$) [2], Hg_2CuTi structure ($F\bar{4}3m$) [19,20], or $B2$ structure ($Pm3m$) [2] depending on composition, and it can be determined by the existence of superlattice reflections and relative intensity of (1 1 1) and (2 0 0) reflections. Weak superlattice (1 1 1) and (2 0 0) reflections can be seen in Fig. 1,

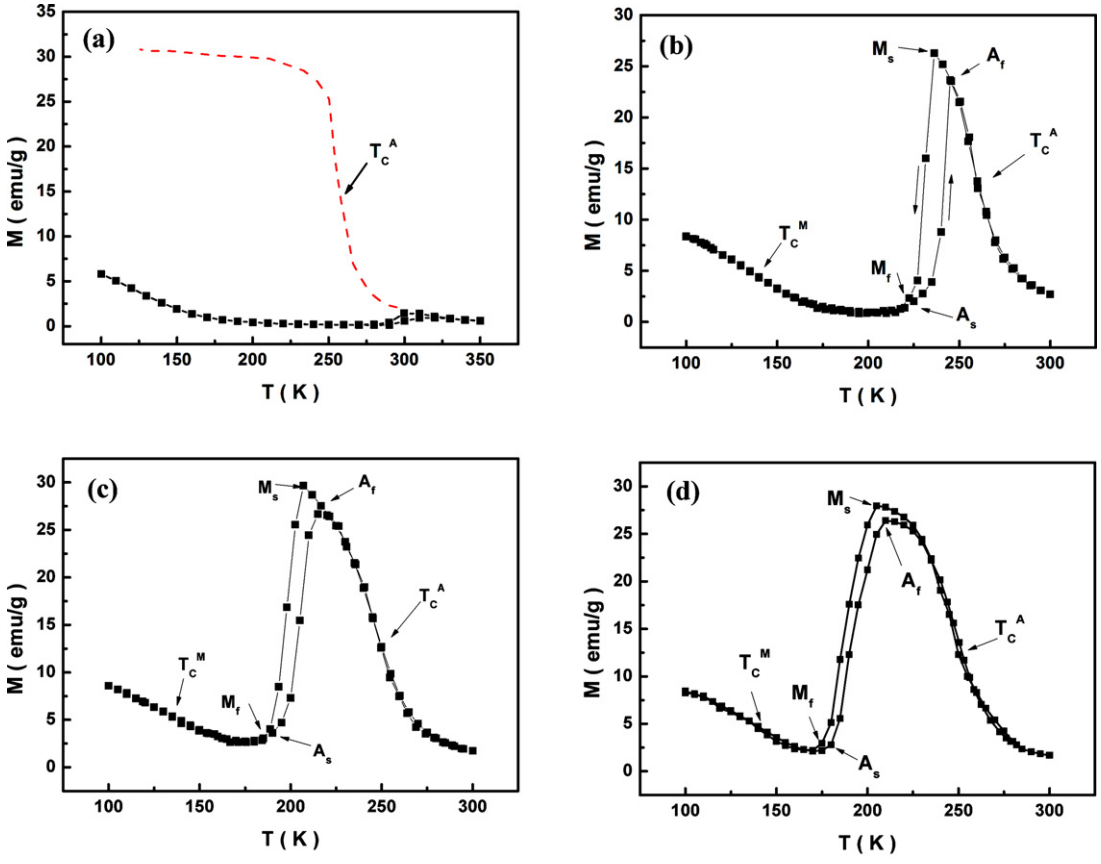

Fig. 3. The temperature dependence of magnetization for $Mn_{50}Ni_{50-x-y}Nb_xSn_9$ alloys in a magnetic field of 1 kOe on heating and cooling (a) $x = 0$; (b) $x = 1$; (c) $x = 2$; (d) $x = 3$.

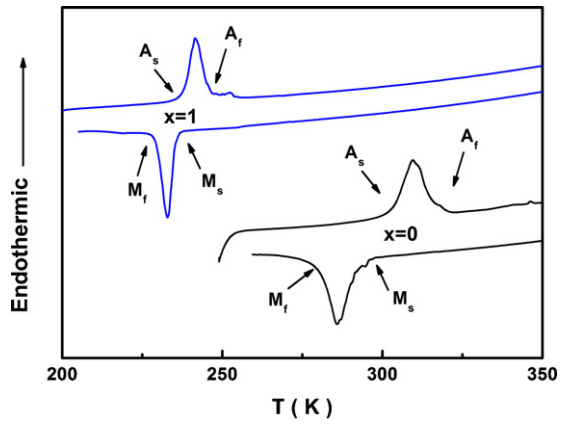

Fig. 4. DSC cooling and heating curves for $Mn_{50}Ni_{50-x-y}Nb_xSn_y$ ($x = 0, 1$; $y = 9$) alloys.

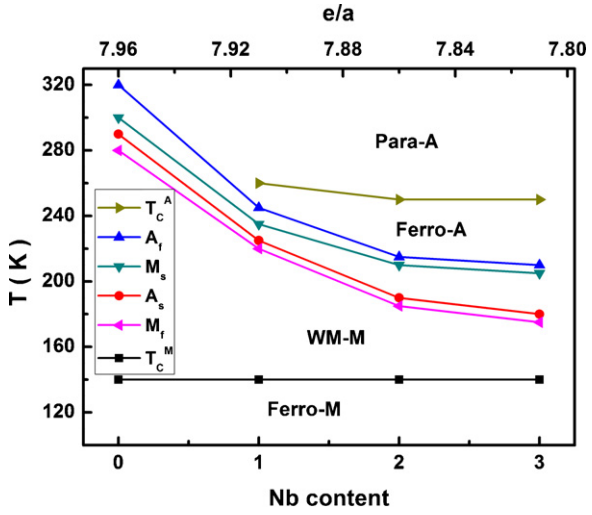

Fig. 5. The characteristic temperatures of phase transitions (M_s, M_f, A_s, A_f, T_C^M, and T_C^A) as a function of Nb content and e/a value for $Mn_{50}Ni_{50-x-y}Nb_xSn_y$ ($x = 0$, 1, 2, 3, $y = 9$) alloys here A and M mean austenitic and martensitic phase, respectively, Para, Ferro, and WM mean paramagnetic, ferromagnetic and weak-magnetic, respectively.

implying the existence of ordered cubic structure. The inset in Fig. 1 shows the zoom of austenite (2 2 0) peaks. It can be seen that (2 2 0) peaks shift toward small angle indicating the expansion of cell volume, which is due to the larger radius of Nb atom (0.208 nm) than Ni atom (0.162 nm). As for $Mn_{50}Ni_{50-x-y}Nb_xSn_y$ ($x = 0, 1, 2$, $y = 10$) alloys, the XRD patterns all show single cubic austenitic phase (not shown here).

Fig. 2 shows the temperature dependence of magnetization $M(T)$ curves for $Mn_{50}Ni_{41}Sn_9$ alloys in a magnetic field of 1 kOe on heating and cooling. On heating from 100 K, the ferromagnetic martensitic phase transforms to weak magnetic martensitic phase with Curie temperature $T_C^M = 104$ K, here the value of T_C^M is determined as the temperature where $|dM/dT|$ is maximum. No thermal hysteresis can be observed near T_C^M between the heating and cooling process, indicating the second order nature of the phase transition. Further increasing temperature induced a small jump of magnetization around 300 K, corresponding to the transition from martensitic phase to austenitic phase. The inset of Fig. 2 shows the $M(H)$ loops of $Mn_{50}Ni_{41}Sn_9$, in which ferromagnetic and weak-magnetic behavior can be observed at 100 and 297 K, respectively. This is consistent with the result of $M(T)$ curves.

It has been reported that three phase transitions occurs in Ni–Mn–X alloys [4–7], i.e. (i) a magnetic transition at T_C^M; (ii) MT, the characteristic temperatures are martensitic start temperature (M_s), martensitic finish temperature (M_f), austenitic start temperature (A_s), austenitic finish temperature (A_f), respectively; (iii) a magnetic transition at T_C^A. Magnetization change across MT (ΔM) is related to phase transition temperatures, and large ΔM can be obtained in the case of $T_C^M < A_s < T_C^A$. For $Mn_{50}Ni_{41}Sn_9$ alloy, our results suggest $T_C^A < A_s$, as shown in Fig. 3(a). Therefore two methods can be used to increase the value of ΔM by tuning the phase transitions in this alloy: (i) increasing the value of T_C^A; (ii) decreasing the value of MT temperatures. It has been proved that the most useful way to increase the value of T_C^A is the addition of Co because Co atoms help the Mn moments align in a ferromagnetic ordering [21]. To decrease the value of MT temperatures, decreasing the value of e/a by 3d transition metal substitution is a commonly used way. Here the substation of Ni by 4d transition-metal Nb was investigated. As shown in Fig. 3(b)–(d), large ΔM across MT can be clearly seen since MT temperatures is reduced and $T_C^M < A_s < T_C^A$ is realized by Nb addition in $Mn_{50}Ni_{50-x-y}Nb_xSn_y$ ($x = 1, 2, 3$, $y = 9$) alloys. As a consequence, large MCE can be expected in these alloys.

In order to further investigate the phase transitions in $Mn_{50}Ni_{50-x-y}Nb_xSn_y$ alloys, DSC cooling and heating curves were measured in the temperature range down to 200 K. Fig. 4 shows the DSC curves for $Mn_{50}Ni_{50-x-y}Nb_xSn_y$ ($x = 0, 1$; $y = 9$) alloys. For both alloys, a well defined endothermic peak appears in the transformation from martensite to austenite during heating, while an exothermic peak is observed in the transformation from austenite to martensite during cooling. The calculated entropy changes across the MT (ΔS) are 33 and 24 J/kg K for $x = 0$ and $x = 1$, respectively. For other alloys, no obvious endothermic and exothermic peaks can be observed down to 200 K (not shown here).

The characteristic temperatures of phase transitions (M_s, M_f, A_s, A_f, T_C^M, and T_C^A) as a function of Nb content and e/a value, which were determined from $M(T)$ curves for $Mn_{50}Ni_{50-x-y}Nb_xSn_y$ ($x = 0, 1, 2, 3$, $y = 9$) alloys, are shown in Fig. 5. Obviously, the values of M_s, M_f, A_s, and A_f decrease with the increase of Nb content. This behavior can be interpreted by the decrease of e/a value since valence electron of Nb is less than Ni. Furthermore, previous investigations in Ga-doped Ni–Mn–In [16] and Ge-doped Ni–Mn–Sn [17] indicated that the MT temperatures increase with the decrease of cell volume. In the case of $Mn_{50}Ni_{50-x-y}Nb_xSn_y$ ($x = 0, 1, 2, 3$, $y = 9$) alloys, Nb addition result in the expansion of cell volume, which may also decrease the values of the MT temperatures. With the increase of Nb content, the value of T_C^M almost keeps constant, while the value of T_C^A shows a slight decrease. This means that the influence of Nb on the exchange interaction is small. Similar results were observed in $Mn_{50}Ni_{50-x-y}Nb_xSn_y$ ($x = 0, 1, 2$, $y = 10$) alloys, as shown in Table 1. It should be noted that, in addition to common way to adjust the MT temperatures in Ni–Mn–X alloys by 3d transition-metal substitution, 4d transition-metal doping may provide an alternative way.

In the systems undergoing first order transition (FOT), where magnetic and structural phase transitions overlap, large entropy change often occurs in respond to temperature and magnetic field due to the involved lattice entropy change. In the determination of entropy change upon the application of magnetic field, i.e. ΔS_M, the most used way is to calculate isothermal magnetization curves using Maxwell relation

$$\Delta S_M(T, H_0) = \mu_0 \int_0^{H_0} \left[\frac{\partial M(T,H)}{\partial T}\right]_H dH \quad (1)$$

For magnetization measurements carried out at constant temperature and discrete H intervals, it can be approximated by

$$\Delta S_M\left(T + \frac{\Delta T}{2}, H_0\right) \approx \frac{\mu_0}{\Delta T}\left[\int_0^{H_0} M(T + \Delta T, H)\, dH - \int_0^{H_0} M(T, H)\, dH\right] \quad (2)$$

Table 1
The values of valence electron concentration (e/a), Curie temperature of martensite (T_C^A), austenitic start temperature (A_s), austenitic finish temperature (A_f), martensitic start temperature (M_s), martensitic finish temperature (M_f), Curie temperature of austenite (T_C^A), and magnetic entropy change (ΔS_M) under the field of 10 kOe for $Mn_{50}Ni_{50-x-y}Nb_xSn_y$ alloys.

$Mn_{50}Ni_{50-x-y}Nb_xSn_y$	e/a	T_C^M (K)	A_s (K)	A_f (K)	M_s (K)	M_f (K)	T_C^A (K)	ΔS_M (J/kg K)
$x=0, y=9$	7.96	140	290	320	300	280		
$x=1, y=9$	7.91	140	225	245	235	220	260	3.8
$x=2, y=9$	7.86	140	190	215	210	185	250	2.5
$x=3, y=9$	7.81	140	180	210	205	175	250	2
$x=0, y=10$	7.9	140	195	225	215	185	280	2.3
$x=1, y=10$	7.85	140	160	180	170	150	275	1.7
$x=2, y=10$	7.8						270	

However, there were some criticisms on the calculation of ΔS_M using Maxwell relation in materials of FOT, and the value of ΔS_M may be overestimated due to hysteresis effect and phase coexistence [22]. Zhang et al. pointed out that the calculation of ΔS_M using Maxwell relation is valid if the applied field is smaller than the critical field [23].

Isothermal magnetization $M(H)$ curves in the temperature range across the MT for $Mn_{50}Ni_{50-x-y}Nb_xSn_y$ alloys were measured. Fig. 6(a) shows $M(H)$ curves of $Mn_{50}Ni_{40}Nb_1Sn_9$ around the MT temperature. No obvious metamagnetic behavior can be observed in the $M(H)$ curves, which means that the critical field for the field-induced metamagnetic transition is larger than 10 kOe. Similar behavior was also observed in $M(H)$ curves for other alloys. Therefore, it should be valid to calculate ΔS_M directly using the $M(H)$ curves due to the high critical field in these alloys. Fig. 6(b) shows the temperature dependence of ΔS_M in the magnetic field of 10 kOe for $Mn_{50}Ni_{50-x-y}Nb_xSn_y$ alloys. Positive peaks indicating inverse MCE can be observed around the MT temperature, and peak position shifts to lower temperature with the increase of Nb content due to the decrease of MT temperatures. The maximum values of ΔS_M in $Mn_{50}Ni_{50-x-9}Nb_xSn_9$ are 3.8, 2.5 and 2.0 J/kg K for $x=1$, 2, and 3, respectively. These values are comparable to the values of Ni_2MnGa [24] and Ni–Mn–Sn [4], which display large MCE near the first-order magnetostructural transition.

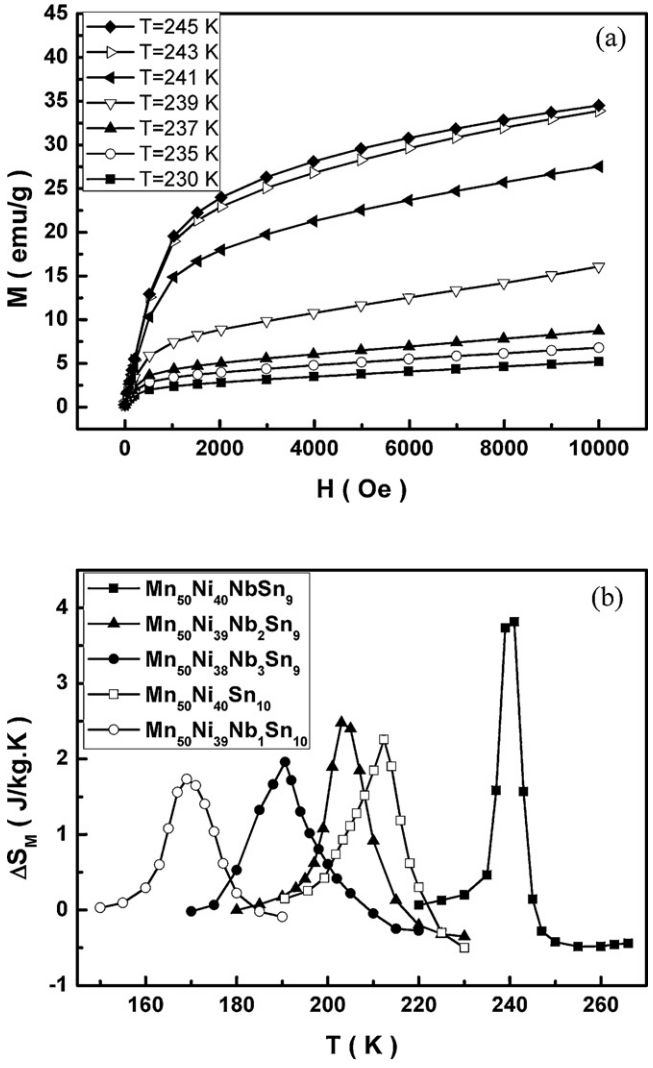

Fig. 6. (a) The isothermal magnetization curves for $Mn_{50}Ni_{40}Nb_1Sn_9$ alloy; (b) the temperature dependence of ΔS_M in the magnetic field of 10 kOe for $Mn_{50}Ni_{50-x-y}Nb_xSn_y$ alloys.

4. Conclusion

In summary, we investigated the influence of 4d transition-metal Nb substitution for Ni in $Mn_{50}Ni_{50-y}Sn_y$ ($x=9$, 10) alloys. With the increase of Nb content, the cell volume of austenitic phase expands due to larger atomic radius of Nb than Ni, the MT temperatures decrease rapidly. The decrease of MT temperatures with Nb doping could be understood by the decrease of e/a. The results imply that the 4d transition-metal doping may provide an alternative way to tailor the martensitic transformation and the MCE in ferromagnetic shape memory alloys.

Acknowledgement

This work was supported by National Natural Science Foundation of China (51001019) and Jiangsu Innovation Project for Undergraduate Student.

References

[1] Y. Sutou, Y. Imano, N. Koeda, T. Omori, R. Kainuma, K. Ishida, K. Oikawa, Appl. Phys. Lett. 85 (2004) 4358.
[2] T. Krenke, M. Acet, E.F. Wassermann, X. Moya, L. Mañosa, A. Planes, Phys. Rev. B 72 (2005) 014412.
[3] T. Krenke, M. Acet, E.F. Wassermann, X. Moya, L. Manosa, A. Planes, Phys. Rev. B 73 (2006) 174413.
[4] T. Krenke, E. Duman, M. Acet, E.F. Wassermann, X. Moya, L. Manosa, A. Planes, Nat. Mater. 4 (2005) 450.
[5] Z.D. Han, D.H. Wang, C.L. Zhang, S.L. Tang, B.X. Gu, Y.W. Du, Appl. Phys. Lett. 89 (2006) 182507.
[6] Z.D. Han, D.H. Wang, C.L. Zhang, B.X. Gu, Y.W. Du, Appl. Phys. Lett. 90 (2007) 042507.
[7] M. Khan, N. Ali, S. Stadler, J. Appl. Phys. 101 (2007) 053919.
[8] S.Y. Yu, Z.H. Liu, G.D. Liu, J.L. Chen, Z.X. Cao, G.H. Wu, B. Zhang, X.X. Zhang, Appl. Phys. Lett. 89 (2006) 162503.
[9] K. Koyama, H. Okada, K. Watanabe, T. Kanomata, R. Kainuma, W. Ito, K. Oikawa, K. Ishida, Appl. Phys. Lett. 89 (2006) 182510.
[10] R. Kainuma, Y. Imano, W. Ito, Y. Sutou, H. Morito, S. Okamoto, O. Kitakami, K. Oikawa, A. Fujita, T. Kanomota, K. Ishida, Nature (Lond.) 439 (2006) 957.
[11] L. Mañosa, X. Moya, A. Planes, O. Gutfleisch, J. Lyubina, M. Barrio, J.L. Tamarit, S. Aksoy, T. Krenke, M. Acet, Appl. Phys. Lett. 92 (2008) 012515.

[12] D.H. Wang, C.L. Zhang, Z.D. Han, H.C. Xuan, B.X. Gu, Y.W. Du, J. Appl. Phys. 103 (2008) 033901.
[13] T. Krenke, E. Duman, M. Acet, X. Moya, L. Manosa, A. Planes, J. Appl. Phys. 102 (2007) 033903.
[14] J. Liu, N. Scheerbaum, D. Hinz, O. Gutfleisch, Appl. Phys. Lett. 92 (2008) 162509.
[15] D.H. Wang, C.L. Zhang, H.C. Xuan, Z.D. Han, J.R. Zhang, S.L. Tang, B.X. Gu, Y.W. Du, J. Appl. Phys. 102 (2007) 013909.
[16] S. Aksoy, T. Krenke, M. Acet, E.F. Wassermann, X. Moya, L. Mañosa, A. Planes, Appl. Phys. Lett. 91 (2007) 241916.
[17] Z.D. Han, D.H. Wang, C.L. Zhang, H.C. Xuan, J.R. Zhang, B.X. Gu, Y.W. Du, Mater. Sci. Eng. B 157 (2009) 40.
[18] H.C. Xuan, K.X. Xie, D.H. Wang, Z.D. Han, C.L. Zhang, B.X. Gu, Y.W. Du, Appl. Phys. Lett. 92 (2008) 242506.
[19] H.Z. Luo, G.D. Liu, Z.Q. Feng, Y.X. Li, L. Ma, G.H. Wu, X.X. Zhu, C.B. Jiang, H.B. Xu, J. Magn. Magn. Mater. 321 (2009) 4063.
[20] Z.H. Liu, Z.G. Wu, X.Q. Ma, W.H. Wang, Y. Liu, G.H. Wu, J. Appl. Phys. 110 (2011) 013916.
[21] R.Y. Umetsu, A. Sheikh, W. Ito, B. Ouladdiaf, K.R.A. Ziebeck, T. Kanomata, R. Kainuma, Appl. Phys. Lett. 98 (2011) 042507.
[22] G.J. Liu, J.R. Sun, J. Shen, B. Gao, H.W. Zhang, F.X. Hu, B.G. Shen, Appl. Phys. Lett. 90 (2007) 032507.
[23] Y.P. Zhang, R.A. Hughes, J.F. Britten, P.A. Dube, J.S. Preston, G.A. Botton, M. Niewczas, J. Appl. Phys. 110 (2011) 013910.
[24] F.X. Hu, B.G. Shen, J.R. Sun, Z.H. Cheng, G.H. Rao, X.X. Zhang, Appl. Phys. Lett. 78 (2001) 3675.